Binding Pocket Response of EDTA Complexes with Alkaline Earth Dications to Stepwise Hydration – Structural Insight from Infrared Spectra‡

Madison M. Foreman,[1] Lane M. Terry,[1] and J. Mathias Weber[1,]*

[1] JILA and Department of Chemistry, University of Colorado at Boulder, UCB 440, Boulder CO 80309, USA

AUTHOR INFORMATION

Corresponding Author

*weberjm@jila.colorado.edu, Tel.: +1-303-492-7841

ABSTRACT. We investigate the microhydration structures of complexes of alkaline earth dications and ethylenediaminetetraacetic acid (EDTA) for up to two water molecules, using cryogenic ion vibrational spectroscopy in concert with density functional theory. The interaction with water shows a clear dependence on the chemical identity of the bound ion. For Mg^{2+}, microhydration mostly involves the carboxylate groups of EDTA and does not entail direct contact with the dication. In contrast, the larger ions (Ca^{2+}, Sr^{2+}, and Ba^{2+}) interact electrostatically with the microhydration environment, and this interaction increases in importance with the size of the ion. This trend reflects the ion position in the EDTA binding pocket, which comes closer to the rim of the pocket with increasing ion size.

TOC GRAPHICS

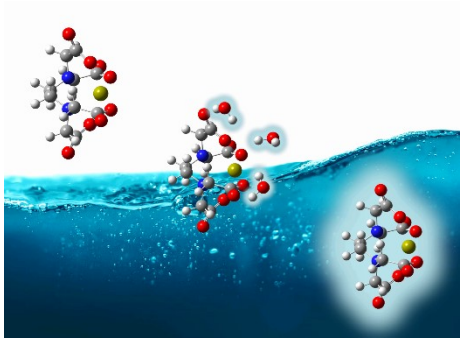

KEYWORDS Chelates; Cryogenic Ion Vibrational Spectroscopy; Host-Guest Complexes; Hydrated Ion Clusters.

Introduction

The interaction of ions with supramolecular structures forming metal ion binding sites is of key importance for many areas of chemical and biochemical processes, such as metal ion sensing,[1] the removal of toxic metal ions in chelating therapy[2-4] and from waste water,[5] and the role of metal ions in biological signaling pathways.[6-7] Binding pockets for metal cations typically consist of a set of polydentate ligands with neutral or anionic binding sites, such as N or O atoms, carbonyl groups, or deprotonated acidic groups (e.g., hydroxyl, thiol, or carboxyl).

In most scenarios where metal ions are bound in such binding sites, water molecules are present as well. Metal bearing complexes can be completely surrounded by water as a solvent (e.g., most metal-chelator complexes), or a small number of water molecules can be present at the mouth of a binding pocket (e.g., in some metal-binding proteins). In some cases, water molecules can even be part of the binding site itself,[8] and the microhydration environment can be part of the mechanism of action for ionophores.[9]

The influence of the chemical environment on the structure and interactions within ion binding sites has received much less attention than the characterization of ion binding sites themselves. This is in part due to the challenges that such investigations encounter in the inherently complex chemical environment in the condensed phase. Infrared (IR) spectroscopy is ideally suited to elucidate structural properties and to obtain insight into intra- and intermolecular forces. However, the spectroscopic response of the solvent and of unbound ions, the fluctuations in the solvation environment of filled binding sites, and heterogeneous line broadening greatly complicate the analysis of condensed phase data and often frustrates efforts to gain a detailed molecular level picture of the influence of solvent molecules on the structures of ion-receptor complexes.

IR spectroscopy of hydrated ion clusters has been a very useful tool to investigate such molecular level details of hydrated ions,[9-25] ranging from small, atomic ions to large ionic complexes. Electrospray ionization can be used together with cryogenic radiofrequency ion traps to prepare hydrated ion clusters of large molecular complexes,[24, 26] and infrared photodissociation spectroscopy of selected cluster ions so prepared circumvents many of the problems mentioned above.

Ethylenediaminetetraacetic acid (EDTA, see Figure 1) is a widely used chelator, which has been invoked previously as a model for Ca^{2+} binding sites in EF hand proteins, such as calmodulin.[27-28] Protein environments often restrict access of water to both the ion and the binding site itself, making the study of microhydrated cluster ions of binding site models with a small, well defined number of water molecules particularly interesting. In a previous paper,[29] we studied complexes of alkaline earth dications with EDTA in vacuo and in bulk aqueous solutions, with exploratory data on water adducts of Ca(II)-EDTA complexes. Here, we extend this work significantly, providing a detailed investigation of the structures of microhydrated cluster ions of the form $[M(II)\cdot EDTA]^{2-}\cdot(H_2O)_{1,2}$ (M = Mg, Ca, Sr, Ba). We interpret the IR photodissociation spectra of these complexes using density functional theory (DFT).

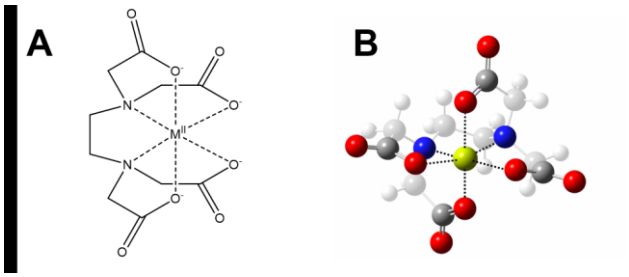

Figure 1. Structure of EDTA chelating an alkaline earth dication. (A) Line drawing of $[M(II)\cdot EDTA]^{2-}$. (B) Calculated structure of $[Ca(II)\cdot EDTA]^{2-}$, highlighting the binding pocket, with red for O, dark gray for C, blue for N, and yellow for Ca. Adapted from [29].

Methods

Experimental

Aqueous stock solutions of $[M(II)\cdot EDTA]^{2-}$ (M = Mg, Ca) were prepared at 5 mM concentration, using disodium salts of EDTA magnesium, EDTA calcium (both from Fisher Scientific). For M = Sr and Ba, approximately equimolar amounts of EDTA and strontium or barium nitrate were dissolved (both from Sigma-Aldrich). The stock solutions were adjusted to pH 12-14 using KOH (Fisher Scientific). For electrospray ionization (ESI), solutions were diluted to 1 mM final concentration, using a 50:50 (by volume) mixture of water and acetonitrile. All chemicals were used without further purification.

The apparatus for cryogenic ion vibrational spectroscopy has been described in detail in earlier work.[30] Gas phase ions of the form $[M(II)\cdot EDTA]^{2-}$ produced by ESI entered the vacuum system through a desolvation capillary held at 75°C. After passing through a skimmer, they were transferred by octopole ion guides and ion optics through a series of differential pumping stages into a cryogenic Paul trap (180 K), where they were cooled in collisions with D_2 buffer gas. Hydrated complex ions with up to two water molecules were formed in three-body collisions with residual water vapor in the trap, originating from the ESI source. After ca. 50 ms cooling time, the contents of the ion trap were injected into the acceleration region of a Wiley-McLaren time-of-flight mass spectrometer. In the first space focus, the target ions were mass-selected using an interleaving comb mass gate[31] and irradiated with the output of a pulsed tunable IR OPO/OPA system (LaserVision, bandwidth ca. 2 cm^{-1}, pulse duration 5-7 ns). Upon photon absorption, photofragments corresponding to the loss of a single water molecule from the hydrated complexes were generated according to

$$[M(II)\cdot EDTA]^{2-}\cdot(H_2O)_n + h\nu \rightarrow [M(II)\cdot EDTA]^{2-}\cdot(H_2O)_{n-1} + H_2O,$$

where n = 1,2. In our earlier work on non-hydrated metal-EDTA complexes,[29] target ions of the composition $[M(II)\cdot EDTA]^{2-}\cdot N_2$ were prepared (20 – 40 K trap temperature), and the loss of the N_2 tag molecule was monitored. Fragment ions were separated from the surviving parent ions using a two-stage reflectron and detected on a double microchannel plate detector. Ion signals were corrected for photon fluence, and several spectra were acquired on different days and averaged to ensure reproducibility and improve signal-to-noise ratio.

In the present work, we only discuss the region of the antisymmetric stretching vibrations of the carboxylate groups of the EDTA moiety (1550 – 1700 cm^{-1}). It is generally desirable to use additional spectral features for structural analysis, such as the analogous OCO symmetric stretching modes or OH stretching features of the water molecules, but experiments in a broader spectral range did not yield additional information. We did not observe any photodissociation signal in the region of the symmetric stretching mode (around 1350 cm^{-1}), probably due to the high binding energy of the water adducts. Exploratory experiments for M = Mg and Ca in the region of the OH stretching vibrations of the water adducts (3100 – 3750 cm^{-1}) show only broad features that do not allow structural identification (see Supporting Information). We ascribe the width of these features to thermal broadening at the trap temperature used here (180 K). Fortunately, the region of the far infrared explored herein encodes structural information about both the carboxylate groups and water adducts, and its features are generally sharp and intense. This enables us to probe for overall complex geometry as well as specific interactions at points of contact between the metal center, chelator, and water adducts.

Computational

Structures and vibrational spectra were calculated using DFT (B3LYP functional[32-33] and def2-TZVPP basis sets[34] for all atoms), similar to our earlier work.[29] All geometries shown here are minimum energy structures obtained through a structural search using many possible starting structures for the water adducts. Infrared spectra for all complexes were calculated based on the harmonic approximation. The frequencies were scaled by 0.977 to match the experimental spectrum for M = Ca in the OCO antisymmetric stretching region. All calculations were performed using Gaussian 16.[35]

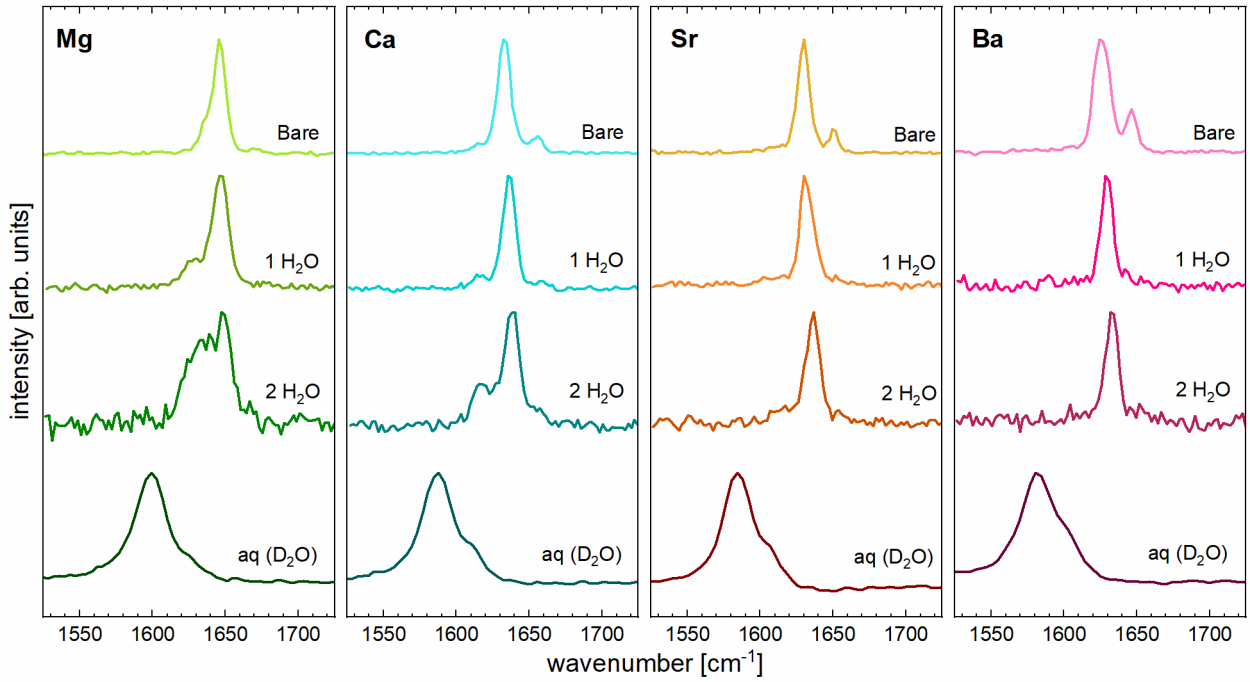

Figure 2. Experimental spectra of bare $[M(II)\cdot EDTA]^{2-}$ complexes (top row), $[M(II)\cdot EDTA]^{2-}\cdot(H_2O)_n$ cluster ions (second and third rows), and bulk solutions of $[M(II)\cdot EDTA]^{2-}$ in D_2O (bottom traces) in the antisymmetric OCO stretching region of the EDTA moiety. The metal ion is indicated in the top panel of each column. Data for bare and fully hydrated complexes, as well as for $[Ca(II)\cdot EDTA]^{2-}\cdot H_2O$, were taken from ref. [29]. The colors in each column turn darker with increasing level of hydration.

Results and Discussion

The antisymmetric OCO stretching region of $[M(II)\cdot EDTA]^{2-}$ complexes is generally characterized by an intense feature between 1625 cm^{-1} and 1650 cm^{-1}, accompanied by a weaker feature 20 cm^{-1} – 25 cm^{-1} higher in energy (see top row in Figure 2). As described in our earlier work,[29] these features encode the different linear combinations of the local OCO oscillators, with the weaker peak in each spectrum being the signature of the radially in-phase combination of the local antisymmetric OCO oscillators (see Supporting Information for an illustration). The other linear combinations of the local OCO oscillators are unresolved under the more intense peak.

In the presence of one or two water molecules (second and third rows in Figure 2), the spectra show consistent trends with increasing solvation, as the weaker peaks at higher energy diminish or disappear, while new features can appear at the low energy side of the intense peaks. These new features are most pronounced for Mg, are clearly observed for Ca, but are practically missing for Sr and Ba. In each of the microhydrated complexes, the coupling of the local carboxylate oscillators is changed by the presence of the water molecules, creating these new spectral patterns. Mixing of the OCO antisymmetric stretching modes with the water bending vibration, which is active in the same region (1625 cm^{-1} to 1675 cm^{-1}), also contributes to the spectra. Each of the resultant mixed modes consists of both CO stretching and water bending motions in varying linear combinations.

Under full hydration (bottom traces in Figure 2), the spectra are significantly red shifted compared to the bare complexes. However, different from the hydrated cluster ions, the spectra return to a similar overall pattern as in the bare complexes, with the totally symmetric combination of the local OCO oscillators now represented as a partially resolved shoulder towards higher energies. This is due in part to the use of D_2O as the solvent in the fully hydrated experiments,

which does not have vibrations that mix with the carboxylate antisymmetric stretching modes. In addition, the much higher temperature and the complete immersion into solvent lead to averaged structures without the distortion of the pocket induced by microhydration. DFT calculations including a polarizable continuum model of water can qualitatively recover this pattern.[29] Curiously, the most intense features in the spectra of the hydrated cluster ions do not exhibit a red shift that would indicate a smooth trend in behavior towards full hydration. Instead, they shift slightly towards higher energies, on average 1-4 cm^{-1} per water molecule, with the weakest shifts for Mg (1 cm^{-1} per water molecule).

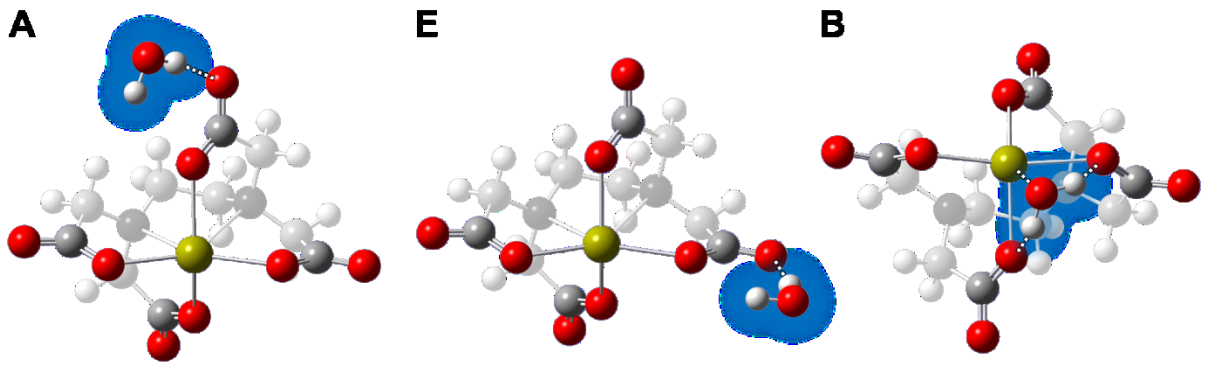

Figure 3. Structural motifs for $[M(II)\cdot EDTA]^{2-}\cdot H_2O$, shown using the calculated structures for M = Ca as an example. A: water molecule H-bonded to an axial ligand; E: water molecule H-bonded to an equatorial ligand; B: water molecule bridging axial and equatorial ligands. Color scheme: M: yellow; O: red; N: blue; C: gray; H: white. Water adducts are highlighted blue and primary H-bonding interactions of the water adduct are shown as dotted lines.

Figure 3 shows the lowest lying structural motifs of calculated structures of $[(M(II)\cdot EDTA]^{2-}\cdot H_2O$ complexes, using M = Ca as an example (see Supporting Information for the other metals). There are three distinct binding geometries for water. In A-type structures, the water molecule forms a strong, linear, single hydrogen bond (H-bond) to one of the O atoms of an axial COO^-

ligand of EDTA. It is weakly interacting with the other O atom of the ligand, but does not form a double H-bond. This is different from the behavior in singly hydrated carboxylate ions, where a single water molecule forms two ionic H-bonds with both O atoms of a COO^- group.[36-39] In all A-type structures, the water molecule is H-bonded to the "outer" O atoms of the carboxylate group, not the "inner" O atom, which binds to the metal. This suggests that the electric field of the metal dication destabilizes the H-bond with the "inner" O atom, despite the fact that this O atom bears more negative charge than the "outer" O atom. In fact, structure optimizations started with an H-bond between the water molecule and the "inner" O atom converged to the structures as shown in Figure 3.

The second structural motif (E) is characterized by the water molecule H-bonding to an equatorial carboxylate ligand, with the interaction between water and the carboxylate group similar to that in structure A.

In the third type of structure (B), the water molecule forms a bridge between an axial and an equatorial ligand, in both cases bound to the "inner" O atoms of each carboxylate group. In this structure, the lone pair on the O atom of the water molecule may also interact with the metal dication in the binding pocket of the complex, but this interaction is strongly dependent on the metal ion (see below).

The central C-C bond of EDTA can serve as a marker for the ion position in the binding pocket (see Supporting Information, Figure S5). Hydration in A or E positions does not appreciably change the position of the ion from the bare geometry. In contrast, hydration in the B position increases that distance for all ions except Mg^{2+}, pulling the ion further to the rim of the pocket. In the Mg complex, the ion is too deep in the pocket for a significant interaction with the water

molecule (see Supporting Information, Table S1). In all cases, the metal-carboxylate distance is greater for the hydrated carboxylate ligand than for the structurally equivalent non-hydrated group.

Interestingly, the isomers change their energetic order for the different metals (see Figure 4). For Mg, the axial and equatorial isomers are isoenergetic, while the bridging isomer is higher in energy. For Ca, all three isomers are isoenergetic, while the bridging isomer is clearly lower in energy for both Sr and Ba. We explain this trend with the fact that the exposure of the ion to the water molecule increases with ion size.[29] While Mg^{2+} is deep inside the binding pocket, Ca^{2+} comes closer to the mouth of the pocket, and Sr^{2+} and Ba^{2+} slightly protrude from the pocket (see Supporting Information for calculated structures). As a result, the larger ions interact electrostatically with the O atom of the water molecule, leading to the stabilization of the bridging isomer compared to A and E isomers.

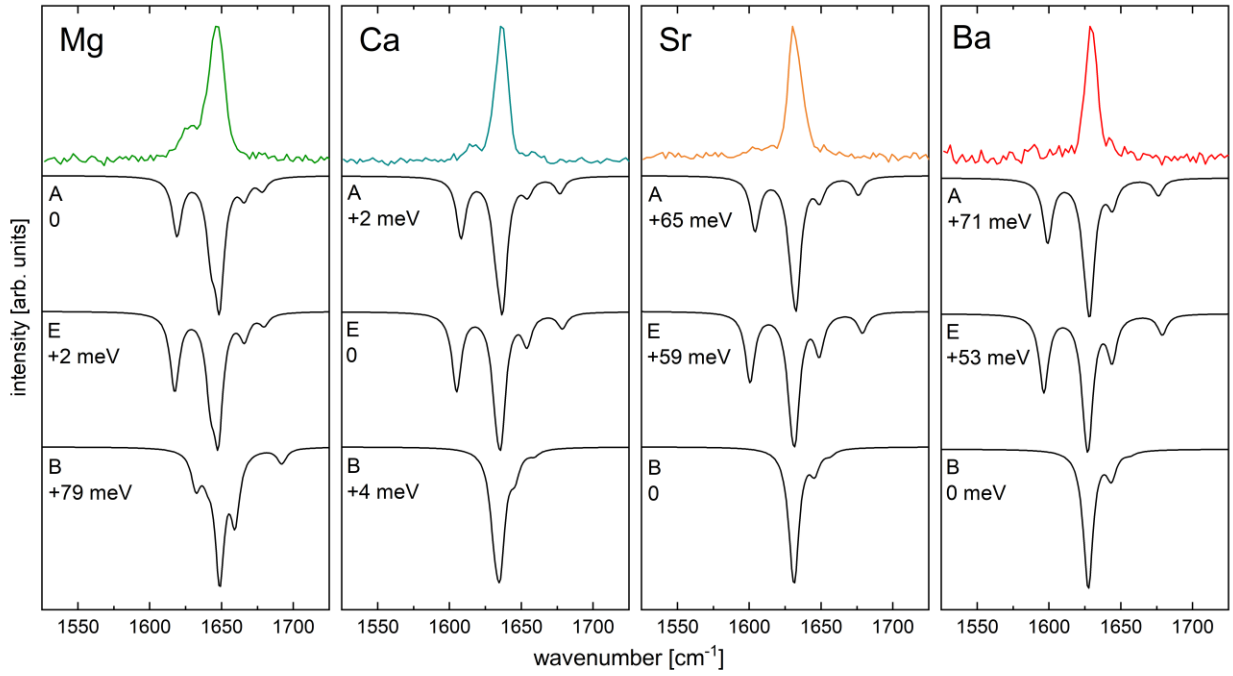

Figure 4. Experimental and calculated spectra for $[M(II)\cdot EDTA]^{2-}\cdot H_2O$ complexes. The identity of each metal is given in the upper left corner of each column. The experimental spectra are shown upright and in a color that varies with the identity of the metal ion, while the calculated spectra are

shown inverted and in black. The calculated spectra are labeled with the hydration isomer (see Figure 3) and its relative energy.

The comparison of experimental and calculated spectra for the different monohydrate isomers is consistent with the calculated energetic order (Figure 4). In light of the negligible calculated energy differences, we assume that $[Mg(II)\cdot EDTA]^{2-}\cdot H_2O$ exists as a mixture of isomers A and E, while all three structural motifs are present for $[Ca(II)\cdot EDTA]^{2-}\cdot H_2O$. The calculated spectra are insufficient to distinguish between isomers A and E. However, the relative intensity of the feature below the most intense peak for M = Ca is lower than for M = Mg, indicating that not only isomers A and E are present.

Based on the calculated patterns of motion for the different OCO stretching modes, we identify the observed new low-frequency features for M = Mg and Ca as the antisymmetric OCO stretching vibrations of hydrated carboxylate groups in A and E isomers. The origin of this red shift is likely found in small geometry changes. For isomer A of the monohydrated Mg-EDTA complex, the calculated OCO bond angle of the hydrated axial carboxylate group is slightly (0.7°) smaller than for the unhydrated axial ligand (128.0°). At the same time, the CO bond length involving the H-bonded O atom is slightly longer (1.0 pm) than the equivalent CO bond on the unhydrated axial ligand (123.8 pm). The E isomer shows similar differences between the hydrated and unhydrated equatorial ligands.

Compared to the unhydrated complexes, this geometry difference changes the coupling between the local antisymmetric OCO stretching oscillators, including their phase relations (see Supporting Information), and all antisymmetric OCO vibrational modes undergo mode mixing with the water bending motion. Calculations predict that the amplitude of the water bend varies among modes and across metal centers. We note that there is no single signature that can be attributed to the

water bending mode due to extensive mixing with the carboxylate antisymmetric stretching modes. For A and E binding sites, the water bending motions are predicted to generally contribute more strongly to modes on the high frequency side of the frequency range studied here, while for B sites, the water bending amplitude cannot be attributed to a more limited set of features.

In the A and E isomers, the new lowest frequency antisymmetric OCO stretching mode is now largely localized on the hydrated carboxylate group, which oscillates radially out of phase with the other three carboxylate ligands (except in the case of M = Mg). The next higher mode, which is an unresolved part of the most intense peak, is largely localized on the three unhydrated carboxylate groups. The second unresolved component of the most intense feature has practically no involvement of the hydrated group. The two highest frequency calculated OCO stretching modes mainly consist of the radially symmetric OCO stretching mode in two linear combinations of opposite phase with the water bending motion in which nearly all of the amplitude of motion is localized to the water bending vibration.

The bridging isomer has other, unique linear combinations of the local OCO oscillators (see Supporting Information), which do not produce features below the most prominent peak in the antisymmetric OCO stretching region. The absence of such features in experimental spectra for Sr and Ba is consistent with the bridging isomer being the dominant structure of the monohydrate for these species, in line with the lower energy of the B isomer compared to A and E.

The dihydrate spectra of $[M(II)\cdot EDTA]^{2-}$ ions roughly continue the trend observed in the monohydrate spectra. The signature on the low-energy side of the main peak grows strongly in relative intensity for M = Mg, and less so for M = Ca, although clearly observable. Apart from the weak blue shift mentioned above, no significant changes are observed going from the mono- to the dihydrate for M = Sr and Ba. Based on the discussion of the calculated monohydrate spectra,

this observation allows formulating the expectation that the metal dependent structural hydration motifs of the monohydrate continues for the dihydrate. We expect the magnesium complex to add the second water molecule in A or E type positions, while a mix of A/E and B type isomers should be populated for the calcium complex with A/E type binding sites somewhat favored, resulting in an increase of the relative intensity of the lower frequency feature. Following this logic, the strontium and barium complexes seem to be adding the second water molecule mainly in another bridging position.

The calculations bear out this expectation. Figure 5 shows the three lowest energy isomers of the dihydrate complexes for each metal (see Supporting Information for higher energy isomers). For M = Mg, the metal atom stays too far buried in the EDTA binding pocket to interact directly with any of the water molecules. The three lowest energy hydration isomers are practically isoenergetic. The two lowest energy structures have the water molecules H-bonding independently to two axial (Mg-AA) or two equatorial (Mg-EE) carboxylate ligands, respectively. The next higher isomer (Mg-AB_{ad}) has a water dimer as a sub-cluster, where one of the water molecules binds to an axial ligand, while the second is adjacent to the first in bridging position to an equatorial ligand. An analogous isomer with a water dimer on an equatorial ligand, bridging to an axial ligand is ca. 60 meV higher in energy (see Supporting Information).

In the complexes with Ca, the picture already changes qualitatively. The three lowest energy hydration isomers are still nearly isoenergetic. However, the two lowest energy structures now exhibit bridging water adducts, stabilized by electrostatic interaction between the metal cation and the oxygen atom of the water. For Sr and Ba complexes, the three lowest energy structures all contain bridging water molecules, and the gap from the lowest to the next higher structure is more pronounced.

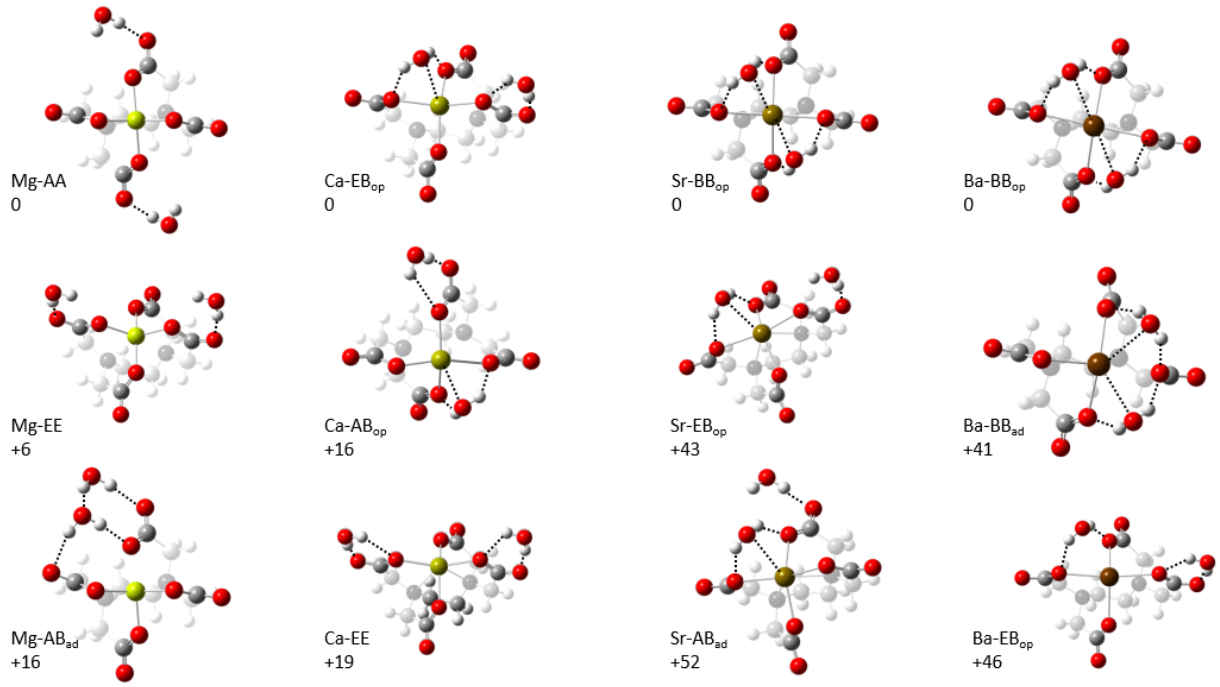

Figure 5. Calculated isomers with the lowest energies in meV for each metal, with the carboxylate ligands, metal atoms, and water molecules highlighted. The labels include the metal and a description of the binding site for each water molecule as defined in Figure 3. Subscripts "op" and "ad" mean that the second water molecule binds to opposite or adjacent carboxylate ligands, respectively. Zero-point corrected energies are given for each structure. Metals are shown in yellow (Mg), dark yellow (Ca), brown (Sr), and dark brown (Ba); O = red; C = grey; H = light grey.

Figure 6 shows the evolution of experimental and calculated spectra illustrated for the cases of Mg and Ba (see Supporting Information for Ca and Sr). Consistent with the experimental spectra for the Mg complexes, the dominant occupation of non-bringing water positions leads to significant intensity increase at the low-energy tail of the antisymmetric OCO stretching region in the calculated spectra, since water molecules in bridging positions lead to the loss of intensity below the dominant peak. The significant population of water molecules in bridging positions for

Ca therefore results in lower relative intensity in this region compared to the Mg complex. Sr and Ba complexes have virtually no intensity below the dominant peak, consistent with the population of only bridging positions, which is in line with the lowest energy isomers.

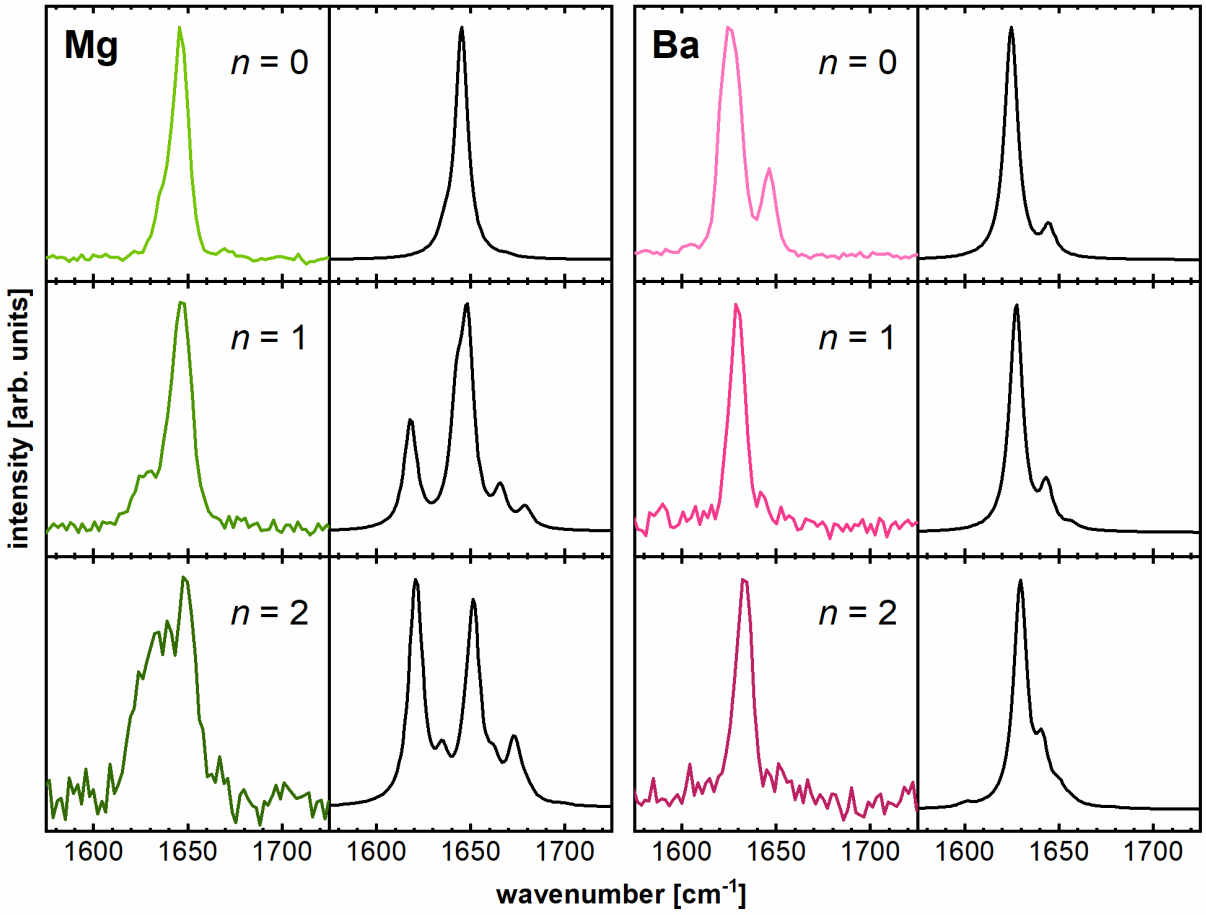

Figure 6. Evolution of IR spectra of $[M{\cdot}EDTA]^{2-}{\cdot}(H_2O)_n$ for M = Mg (left double column) and Ba (right double column). The left panels in each double column are experimental data, the right columns are the Boltzmann-weighted sum of the calculated spectra for the isomers with relative energies of 46 meV or less (corresponding to isomers with at least 5% of the ground state population at 180 K) of each cluster size (given in the experimental columns). The calculated spectra are scaled to match the highest intensity feature of the corresponding experimental spectrum.

Conclusions

In summary, infrared spectra of mass-selected $[M(II)\cdot EDTA]^{2-}\cdot(H_2O)_n$ complexes (M = Mg, Ca, Sr, Ba; n = 0, 1, 2) and of the same $[M(II)\cdot EDTA]^{2-}$ species in solution were measured and compared in the OCO antisymmetric stretching region. The singly and doubly hydrated complexes exhibit small frequency shifts in the main spectral features (1–5 cm^{-1}) from their unhydrated positions, and new signatures grow in for M = Mg and Ca. These new peaks correspond to water molecules forming hydrogen bonds to the axial and equatorial carboxylate groups of the EDTA chelator. The spectra of M = Sr and Ba consist of only one high-intensity peak, consistent with preferentially binding water adducts in a bridging motif. While Mg^{2+} bound by EDTA does not have significant contact with the microhydation environment, the larger ions (Ca^{2+}, Sr^{2+}, and Ba^{2+}) interact electrostatically with water molecules bound to the pocket, and this interaction increases in importance with the size of the ion. This trend exacerbates the intrinsic dependence of the ion position in the EDTA binding pocket on the chemical identity of the ion, increasing the exposure of the larger ions to the microhydration environment. It persists towards full hydration, demonstrating the role of the solvation environment in shaping the structural and binding characteristics of the binding pocket.

ASSOCIATED CONTENT

Supporting Information. Spectra of $[M(II)\cdot EDTA]^{2-}\cdot H_2O$ in the mid-IR spectral region for M = Mg and Ca; patterns of motion of the antisymmetric OCO vibrational modes; ion position in the binding pocket of unhydrated EDTA complexes; calculated structures of $[(M(II)\cdot EDTA]^{2-}\cdot H_2O$ complexes; ion position in the binding pocket of unhydrated EDTA complexes; selected structural properties of $[M(II)\cdot EDTA]^{2-}\cdot H_2O$ complexes; hydration dependent evolution of IR spectra of

$[M \cdot EDTA]^{2-} \cdot (H_2O)_n$ for all metals; calculated dihydrate isomers for all metals; atomic coordinates of $[M(II) \cdot EDTA]^{2-} \cdot H_2O$ complexes.

AUTHOR INFORMATION

Corresponding Author

*weberjm@jila.colorado.edu; Tel.: +1-303-492-7841

Notes

‡ Based on: Madison M. Foreman, Study on Metal-Ligand Interactions: Infrared Ion Spectroscopy of Coordination Compounds, PhD Thesis (2023) University of Colorado Boulder.

The authors declare no competing financial interests.

ACKNOWLEDGMENT

J.M.W. gratefully acknowledges support from the U. S. National Science Foundation under awards no. CHE-1764191, CHE-2154271 and PHY-1734006. This work utilized resources from the University of Colorado Boulder Research Computing Group, which is supported by the National Science Foundation (awards ACI-1532235 and ACI-1532236), the University of Colorado Boulder, and Colorado State University.

REFERENCES

(1) Valeur, B.; Leray, I. Design Principles of Fluorescent Molecular Sensors for Cation Recognition. *Coord. Chem. Rev.* **2000,** *205*, 3-40.

(2) Aaseth, J.; Jacobsen, D.; Andersen, O.; Wickstrøm, E. Treatment of Mercury and Lead Poisonings with Dimercaptosuccinic Acid and Sodium Dimercaptopropanesulfonate. A Review. *Analyst* **1995,** *120*, 853-854.

(3) Andersen, O. Principles and Recent Developments in Chelation Treatment of Metal Intoxication. *Chem. Rev.* **1999,** *99*, 2683-2710.

(4) Harrington, J. M.; Boyd, W. A.; Smith, M. V.; Rice, J. R.; Freedman, J. H.; Crumbliss, A. L. Amelioration of Metal-Induced Toxicity in Caenorhabditis Elegans: Utility of Chelating Agents in the Bioremediation of Metals. *Toxicol. Sci.* **2012,** *129*, 49-56.

(5) Han, M.; He, J.; Wei, X.; Li, S.; Zhang, C.; Zhang, H.; Sun, W.; Yue, T. Deep Purification of Copper from Cu(II)-EDTA Acidic Wastewater by Fe(III) Replacement/Diethyldithiocarbamate Precipitation. *Chemosphere* **2022,** *300*, 134546.

(6) Ghosh, A.; Greenberg, M. E. Calcium Signaling in Neurons: Molecular Mechanisms and Cellular Consequences. *Science* **1995,** *268*, 239-247.

(7) Bers, D. M. Calcium Cycling and Signaling in Cardiac Myocytes. *Annu. Rev. Physiol.* **2008,** *70*, 23-49.

(8) Gifford, J. L.; Walsh, M. P.; Vogel, H. J. Structures and Metal-Ion-Binding Properties of the Ca^{2+}-Binding Helix-Loop-Helix Ef-Hand Motifs. *Biochem. J.* **2007,** *405*, 199-221.

(9) Sato, E.; Hirata, K.; Lisy, J. M.; Ishiuchi, S.; Fujii, M. Rethinking Ion Transport by Ionophores: Experimental and Computational Investigation of Single Water Hydration in Valinomycin-K^+ Complexes. *J. Phys. Chem. Lett.* **2021,** *12*, 1754-1758.

(10) Lisy, J. M. Spectroscopy and Structure of Solvated Alkali-Metal Ions. *Int. Rev. Phys. Chem.* **1997,** *16*, 267-289.

(11) Robertson, W. H.; Johnson, M. A. Molecular Aspects of Halide Ion Hydration: The Cluster Approach. *Annu. Rev. Phys. Chem.* **2003,** *54*, 173-213.

(12) Bush, M. F.; Saykally, R. J.; Williams, E. R. Hydration of the Calcium Dication: Direct Evidence for Second Shell Formation from Infrared Spectroscopy. *ChemPhysChem* **2007,** *8*, 2245-2253.

(13) Jockusch, R. A.; Lemoff, A. S.; Williams, E. R. Effect of Metal Ion and Water Coordination on the Structure of a Gas-Phase Amino Acid. *J. Am. Chem. Soc.* **2001,** *123*, 12255-12265.

(14) Pankewitz, T.; Lagutschenkov, A.; Niedner-Schatteburg, G.; Xantheas, S. S.; Lee, Y. T. Infrared Spectrum of $NH_4^+(H_2O)$: Evidence for Mode Specific Fragmentation. *J. Chem. Phys.* **2007,** *126*, 074307.

(15) Beyer, M. K. Hydrated Metal Ions in the Gas Phase. *Mass Spectrom. Rev.* **2007,** *26*, 517-541.

(16) Nagornova, N. S.; Rizzo, T. R.; Boyarkin, O. V. Interplay of Intra- and Intermolecular H-Bonding in a Progressively Solvated Macrocyclic Peptide. *Science* **2012,** *336*, 320-323.

(17) Asmis, K. R.; Neumark, D. M. Vibrational Spectroscopy of Microhydrated Conjugate Base Anions. *Acc. Chem. Res.* **2012,** *45*, 43-52.

(18) Rijs, A. M.; Oomens, J. Ir Spectroscopic Techniques to Study Isolated Biomolecules. *Top. Curr. Chem.* **2015,** *364*, 1-42.

(19) Rizzo, T. R.; Boyarkin, O. V., Cryogenic Methods for the Spectroscopy of Large, Biomolecular Ions. In *Gas-Phase Ir Spectroscopy and Structure of Biological Molecules*, Rijs, A. M.; Oomens, J., Eds. 2015; Vol. 364, pp 43-97.

(20) Wada, K.; Kida, M.; Muramatsu, S.; Ebata, T.; Inokuchi, Y. Conformation of Alkali Metal Ion-Calix[4]Arene Complexes Investigated by Ir Spectroscopy in the Gas Phase. *Phys. Chem. Chem. Phys* **2019,** *21*, 17082-17086.

(21) Wolk, A. B.; Leavitt, C. M.; Garand, E.; Johnson, M. A. Cryogenic Ion Chemistry and Spectroscopy. *Acc. Chem. Res.* **2014,** *47*, 202-210.

(22) Blom, M. N.; Compagnon, I.; Polfer, N. C.; von Helden, G.; Meijer, G.; Suhai, S.; Paizs, B.; Oomens, J. Stepwise Solvation of an Amino Acid: The Appearance of Zwitterionic Structures. *J. Phys. Chem. A* **2007,** *111*, 7309-7316.

(23) Jagoda-Cwiklik, B.; Jungwirth, P.; Rulisek, L.; Milko, P.; Roithova, J.; Lemaire, J.; Maitre, P.; Ortega, J. M.; Schröder, D. Micro-Hydration of the $MgNO_3^+$ Cation in the Gas Phase. *ChemPhysChem* **2007,** *8*, 1629-1639.

(24) Garand, E. Spectroscopy of Reactive Complexes and Solvated Clusters: A Bottom-up Approach Using Cryogenic Ion Traps. *J. Phys. Chem. A* **2018,** *122*, 6479-6490.

(25) Yang, Y.; Johnson, C. J. Hydration Motifs of Ammonium Bisulfate Clusters of Relevance to Atmospheric New Particle Formation. *Faraday Disc.* **2019,** *217*, 47-66.

(26) Zviagin, A.; Kopysov, V.; Boyarkin, O. V. Gentle Nano-Electrospray Ion Source for Reliable and Efficient Generation of Microsolvated Ions. *Rev. Sci. Instrum.* **2022,** *93*.

(27) Edington, S. C.; Baiz, C. R. Vibrational Relaxation in EDTA Is Ion-Dependent. *J. Phys. Chem. A* **2018,** *122*, 6585-6592.

(28) Edington, S. C.; Gonzalez, A.; Middendorf, T. R.; Halling, D. B.; Aldrich, R. W.; Baiz, C. R. Coordination to Lanthanide Ions Distorts Binding Site Conformation in Calmodulin. *Proc. Natl. Acad. Sci.* **2018,** *115*, E3126-E3134.

(29) Foreman, M. M.; Weber, J. M. Ion Binding Site Structure and the Role of Water in Alkaline Earth EDTA Complexes. *J. Phys. Chem. Lett.* **2022,** *13*, 8558-8563.

(30) Xu, S.; Gozem, S.; Krylov, A. I.; Christopher, C. R.; Mathias Weber, J. Ligand Influence on the Electronic Spectra of Monocationic Copper-Bipyridine Complexes. *Phys. Chem. Chem. Phys* **2015,** *17*, 31938-31946.

(31) Stoermer, C. W.; Gilb, S.; Friedrich, J.; Schooss, D.; Kappes, M. M. A High Resolution Dual Mass Gate for Ion Separation in Laser Desorption/Ionization Time of Flight Mass Spectrometry. *Rev. Sci. Instrum.* **1998,** *69*, 1661-1664.

(32) Becke, A. D. Density-Functional Thermochemistry .3. The Role of Exact Exchange. *J. Chem. Phys.* **1993,** *98*, 5648-5652.

(33) Lee, C. T.; Yang, W. T.; Parr, R. G. Development of the Colle-Salvetti Correlation-Energy Formula into a Functional of the Electron-Density. *Phys. Rev. B* **1988,** *37*, 785-789.

(34) Weigend, F.; Ahlrichs, R. Balanced Basis Sets of Split Valence, Triple Zeta Valence and Quadruple Zeta Valence Quality for H to Rn: Design and Assessment of Accuracy. *Phys. Chem. Chem. Phys.* **2005,** *7*, 3297-3305.

(35) Frisch, M. J.; Trucks, G. W.; Schlegel, H. B.; Scuseria, G. E.; Robb, M. A.; Cheeseman, J. R.; Scalmani, G.; Barone, V.; Petersson, G. A.; Nakatsuji, H. et al. *Gaussian 16 Rev. C.01*, Wallingford, CT, 2016.

(36) Robertson, W. H.; Price, E. A.; Weber, J. M.; Shin, J. W.; Weddle, G. H.; Johnson, M. A. Infrared Signatures of a Water Molecule Attached to Triatomic Domains of Molecular Anions: Evolution of the H-Bonding Configuration with Domain Length. *J. Phys. Chem. A* **2003,** *107*, 6527-6532.

(37) Goebbert, D. J.; Wende, T.; Bergmann, R.; Meijer, G.; Asmis, K. R. Messenger-Tagging Electrosprayed Ions: Vibrational Spectroscopy of Suberate Dianions. *J. Phys. Chem. A* **2009,** *113*, 5874-5880.

(38) DeVine, J. A.; Debnath, S.; Li, Y. K.; McCaslin, L. M.; Schöllkopf, W.; Neumark, D. M.; Asmis, K. R. Infrared Photodissociation Spectroscopy of D_2-Tagged $CH_3CO_2^-(H_2O)_{0-2}$ Anions. *Mol. Phys.* **2020,** *118*, e1749953.

(39) Mitra, S.; Denton, J. K.; Kelleher, P. J.; Johnson, M. A.; Guasco, T. L.; Choi, T. H.; Jordan, K. D. Water Network Shape-Dependence of Local Interactions with the Microhydrated $-NO_2^-$ and $-CO_2^-$ Anionic Head Groups by Cold Ion Vibrational Spectroscopy. *J. Phys. Chem. A* **2022,** *126*, 2471-2479.

TOC GRAPHICS